J. Membrane Biol. 208, 171–182 (2005)
DOI: 10.1007/s00232-005-0828-6

The Journal of
Membrane
Biology

Comparison of Responses to Electrical Stimulation and Whisker Deflection Using Two Different Voltage-sensitive Dyes in Mouse Barrel Cortex in Vivo

E.F. Civillico, D. Contreras
[1]Department of Neuroscience, University of Pennsylvania School of Medicine, 215 Stemmler Hall, Philadelphia, PA 19104, USA

Received: 12 December 2005

Abstract. We examined the spatial structure of noise in optical recordings made with two commonly used voltage-sensitive dyes (RH795 and RH1691) in mouse barrel cortex in vivo, and determined that the signal-to-noise ratio of the two dyes was comparable when averaging over barrel-sized areas, or at single pixels distant from large blood vessels. We examined the spatiotemporal development of whisker- and electrically-evoked optical responses by quantifying the area of activated cortical surface as a function of time. Whisker and electrical stimuli activated cortical areas between 0.2–2.0 mm^2 depending on intensity. More importantly, both types of activation recruited cortical area at similar rates and showed a linear relationship between the maximal activated area and the peak rate of increase of the activated area. We propose a general rule of supragranular cortical activation in which the initial spreading speed of the response determines the total activated area, independent of the type of activation. Finally, despite comparable single-response kinetics, we observed greater paired-pulse depression of whisker-evoked responses relative to electrically-evoked responses.

Key words: VSD — Fluorescence — Imaging — RH795 — RH1691

Introduction

The rodent SI whisker, or "barrel," cortex is an experimentally accessible primary sensory cortical area, with a well-characterized columnar organization (Woolsey & Van der Loos, 1970). An array of barrel-shaped structures in layer 4, each associated primarily with one whisker on the contralateral face, can be visualized by staining for the enzyme cytochrome oxidase. The cortical map formed by this array of barrels is topographically organized with respect to the whiskers. Functional and anatomical projections from the whisker-associated barrels extend vertically throughout the entire cortical column, and barrel-columns have horizontal projections into many neighboring barrel-columns. The combination of topological clarity with physiological complexity has made this sensory map an attractive system for imaging cortical function. Both intrinsic signal (Masino et al., 1993; Goldreich, Peterson & Merzenich, 1998; Erinjeri & Woolsey, 2002; Devor et al., 2003) and voltage-sensitive dye (VSD) imaging (Kleinfeld & Delaney, 1996; Petersen, Grinvald & Sakmann, 2003a; Petersen et al., 2003b) have been successfully used in barrel cortex in vivo to describe the spread of neural activity associated with responses to whisker deflection.

The use of physiologically realistic stimuli, i.e., controlled movements of the whiskers, to stimulate barrel cortex is obviously fundamental to understanding its computational function. However, the circuit properties of cortical networks may also be probed using direct epicortical electrical stimulation. Such stimulation has a long history of use to explore network dynamics, both in vivo (Morin & Steriade, 1981; Timofeev, Contreras & Steriade, 1996; Contreras, Durmuller & Steriade, 1997) and in vitro (Gil, Connors & Amitai, 1997, Yuste, Tank & Kleinfeld, 1997). Experiments in which electrical stimuli are delivered to one location while recordings are made from another have revealed functional projections between areas, as well as frequency- and modulation-dependent properties of thalamocortical (Gil et al., 1997, 1999) and corticocortical (Contreras & Llinas, 2001) connections. Delivery of a brief (100 μs)

Correspondence to: D. Contreras; email: diegoc@mail.med.upenn.edu

electrical stimulus elicits a barrage of action potentials from cells and axons located in the vicinity of the electrode (the presynaptic or direct response). Subsequently, activity developing over tens or hundreds of milliseconds following the stimulus in the recorded area (the postsynaptic response) is indicative of the strength and nature of the connection from the area activated directly. When optical recording methods are used, a large amount of data is generated by such a stimulus, since the response may be observed at thousands of discrete locations. The optical response is thought to be generated mainly by the dendrites postsynaptic to the cells excited directly (Yuste et al., 1997; Contreras & Llinas, 2001), although detailed stereological analysis reveals that far more axonal than dendritic membrane per unit of volume is present in the neuropil of layers 2 and 3 (C. Avendano, *personal communication*).

The use of electrical stimuli carries the caveat that such stimuli may initiate combinations of synaptic events that would never occur in response to physiological stimuli, possibly by activating large populations of cortical cells at unrealistic strengths. Here, using voltage-sensitive dyes, we compare optical recordings in which the whiskers were stimulated, delivering excitation to the cortex via thalamic pathways, with recordings in which electrical stimuli of varying amplitude activated cortical tissue directly. We compare the responses with respect to the amount of cortical area activated and the speed with which the area is activated. We also explore spatial considerations in the signal-to-noise properties of two commonly used potentiometric membrane-bound dyes, RH795 and RH1691, as seen in our studies in adult mouse barrel cortex in vivo.

Materials and Methods

Tissue Preparation

Results are based on 37 adult C57 mice (7–10 weeks old, 20 g). Experiments were selected for analysis based on the following criteria: (i) homogeneous staining of the preparation as judged by visual inspection of the baseline image (14-bit) obtained at the beginning of each recording, (ii) stability of the optical responses throughout the experimental session, (iii) stability of the EEG pattern recorded from the same electrodes used for electrical stimulation, and (iv) stability of the evoked local field potential (LFP) responses recorded by electrodes adjacent to the stimulating one.

Mice were deeply anesthetized with ketamine-xylazine (100 mg/kg i.p., 20 mg/kg i.p. respectively) and mounted in a stereotaxic apparatus. Supplemental anesthesia (25 mg/kg, 5 mg/kg) was administered as necessary to maintain cortical slow oscillations and weak or absent foot withdrawal reflex. A craniotomy was made, which extended in the anterior-posterior direction from bregma to 2 mm posterior of bregma, and in the mediolateral direction from 2–4 mm lateral to the midline. In most animals this was sufficient to expose most of the whisker representation in SI cortex. The dura was resected over the entire craniotomy.

Once electrodes were inserted, hand stimulation of the whiskers with audio feedback from the cortical field potentials was used to determine the approximate location of the electrodes within the PMBSF. This information was used to determine the whiskers most suitable for VSD imaging.

Following Kleinfeld and Delaney (1996), a 1 mm^3 piece of gelfoam (Upjohn Pharmacia) was soaked in a warm solution of the voltage-sensitive dye RH795 (Molecular Probes, Eugene, OR, 1 mg/mL) or RH1691 (Optical Imaging, Mountainside, NJ, 1 mg/mL) in 0.9% saline and placed on the exposed cortex. Additional dye was added as necessary to keep the gelfoam soaked for 1.5 hours. After staining and before recording, the exposed surface of the brain was generously washed with saline to remove unbound dye. Throughout the experiment the brain surface was rinsed with saline to prevent desiccation.

Electrophysiological Recordings

To record LFP and deliver electrical stimulation, we manufactured arrays of 3 or 4 pairs of tungsten electrodes (FHC, Bowdoinham, ME). Electrodes in each pair had a vertical tip separation of 0.5 mm and the distance between pairs in the array was 0.75 mm. For each experiment one array was advanced into the cortex at the lateral edge of the craniotomy, normal to the cortical surface. The array was advanced under microscope visualization so that the upper electrodes were just under the pial surface.

Recordings of cortical local field potentials (LFP) were made in bipolar configuration between the pial surface and the depth of the cortex. Such an arrangement ensures that the cortical dipole is spanned and facilitates the interpretation of LFP recordings. The polarity of the bipolar LFP was set so that the initial response from the depth electrode was negative. As established with intracellular recordings in vivo (Creutzfeldt, Watanabe & Lux, 1966; Contreras & Steriade, 1995), the initial EPSP in response to cortical stimulation is seen in the LFP as a negative deflection at depth, and is reversed at the surface of the cortex. The IPSP which follows the EPSP in most cortical cells is reflected in the LFP as a surface-negative, depth-positive wave. We set the polarity of the bipolar recording to match that of the depth electrode and compared the negative LFP response, reflecting an EPSP, to the optical signal, reflecting population intracellular membrane potential in the supragranular layers. The field potential responses were monitored throughout the experiment on at least one additional cortical electrode to ensure the continuing health of the cortex. The signal from the electrodes was band-pass filtered between 0.1 and 30 Hz to obtain LFP recordings, and between 300 and 10,000 Hz to obtain multiunit activity (MUA).

Staining

RH795 (Grinvald et al., 1994; Obaid et al., 2004) and RH1691 (Shoham et al., 1999) are potentiometric styryl dyes, which attach to cell membranes and show an increase (RH1691) or decrease (RH795) in fluorescence on a microsecond time scale in response to membrane depolarization. For consistency with convention, all VSD responses shown here are oriented so that positive-going deflections indicate depolarization. Potentiometic dyes are linear indicators of membrane potential V_m over physiological ranges (Cohen & Salzberg, 1978; Cohen, Salzberg & Grinvald, 1978; Salzberg et al., 1983).

When applied topically in vivo, the dyes stain the supragranular cortical layers most intensely (Kleinfeld & Delaney, 1996; Petersen et al., 2003a). The dye is taken up preferentially by dendrites and cell bodies; however, layers 2/3 are primarily neuropil (Grinvald et al., 1994; Yuste et al., 1997; Contreras & Llinas, 2001).

Some contribution comes also from glial cells (Konnerth, Obaid & Salzberg, 1987; Salzberg, 1989).

Optical Recordings

A modified upright microscope (Olympus, BX50WI) was mounted on a surgical table, on rails to allow the optical apparatus to slide away for surgery and electrode placement. Epi-illumination was provided by a 12 V halogen lamp. For RH795, excitation light was bandpass-filtered at 540 ± 20 nm; light emitted from the preparation was long pass-filtered below 600 nm. For RH1691, excitation light was bandpass-filtered at 620 ± 30 nm; light emitted from the preparation was long pass-filtered below 665 nm. The optical signal was collected with a CCD camera (MiCam01, BrainVision, Japan) with a detector array of 96 × 64 pixels (87 × 60 imageable) at a frame rate of 250 Hz (4 ms/frame). The microscope objective was 4× (N.A. = 0.28, Olympus, Japan), resulting in an imageable area of 1.5 by 2.0 mm and a pixel size of 22 by 22 μm (484 μm^2). Optical recording was controlled by the MiCam software.

Electrical Stimulation

Electrical stimuli consisted of single 100 μs pulses of 0.1–0.3 mA intensity delivered through the recording electrodes in a bipolar configuration.

Cytochrome Oxidase Histology

At the conclusion of an imaging experiment, 2 additional fiducial marks were made by advancing a single electrode into the cortex. Reference images in register with the VSD recordings were taken with these new marks. Animals were perfused with 4% paraformaldehyde in 0.1 M sodium phosphate buffer (PBS). Brains were postfixed overnight in the same fixative and the cortex was flattened by pressing gently between two clean microscope slides submerged in PBS. One hundred micron thick tangential sections were cut in a vibratome (Vibratome 1000-plus). In order to reveal the barrels, tissue was treated with 3,3′-Diaminobenzidine (DBA, Sigma D-5905) and Cytochrome C from horse heart (Sigma C-2506) according to the original protocol from Wong-Riley (1979) with some modifications. Briefly, sections were washed in 0.1 M PBS (3 × 10 min) at room temperature and incubated in a mixture of 0.1 M PBS with 10% methanol (Fisher Scientific BP1105-1) and 1% hydrogen peroxide (Sigma H-1009) for 15 minutes at room temperature, washed again in PBS (3 × 10 min) and kept in the dark, shaking overnight at 4°C in 0.1 M PBS containing 4 g sucrose, 50 mg DBA (Sigma) and 30 mg of cytochrome oxidase per 100 ml of phosphate buffer (PB). The following day, tissue was washed in PBS, mounted in subbed glass slides, dehydrated and coverslipped.

Barrel Binning

The tracks left by the field potential electrodes, in combination with the additional fiducial marks made at the end of the experiment, were used to align the barrel outlines from histology with the fractional fluorescence images. This allowed binning of pixels into signals corresponding to the average activity within barrel-columns while also increasing the signal-to-noise ratio.

Data Analysis

Optical data was collected as differential fluorescence and divided by a reference image to produce fractional fluorescence ($\Delta F/F$) data, which was used for all analyses and figures. Post-processing consisted of averaging over trials. For clarity of presentation some recordings were spatially smoothed with a 100 μm × 100 μm flat kernel; however, all quantification was performed on unsmoothed data. All analysis was done with custom routines written in Igor Pro (Wavemetrics, Lake Oswego, OR).

Thresholding and Visualization

For each recording, the baseline noise was quantified by obtaining the standard deviation (SD) at each pixel during 100 ms prior to the stimulus, and then plotting the distribution of these SDs. This distribution was always unimodal, with the peak representing the most common SD over the image. For quantification of activated areas as a function of time, a threshold of twice this value was used.

Dye Penetration Depth

To verify the source of the VSD signal, for several representative experiments we cut coronal slices immediately following perfusion, and visualized them with the same optical apparatus. A typical example is shown in Fig. 1*A*, in which three CCD images have been overlapped to produce a complete image of the extent of dye spread at the anterior-posterior midpoint of the craniotomy. In keeping with the reports of others (Kleinfeld & Delaney 1996, Petersen & Sakmann 2003), we observed an even penetration of the dye across the craniotomy, down to 500 μm, which we consider to include all of layers 2/3 and possibly some of layer 4. The lower border of the cortex, determined by superposition of a nonfluorescent image of the same slice, is shown in white.

Results

Comparison of Signal-to-noise Ratio: RH795 vs RH1691

We compared the noise in recordings made with two commonly used voltage-sensitive dyes by plotting the standard deviation over 100 ms of unstimulated recording at each pixel against the square root of the baseline fluorescence at that pixel. On such a plot, a good fit to a line indicates that the noise is dominated by the photon shot noise intrinsic to any optical recording method. Figure 1*B* shows the results of this plot for ten representative experiments, five with RH1691 and five with RH795. The *x*-axis covers the entire dynamic range of the camera, though not linearly, due to the square-root operation. The plot shows that despite identical handling and application of the dyes, as a rule we observed brighter staining in adult mouse cortex with RH795, and this brighter staining was associated with a lower variance in the baseline signal. The plot of standard deviation against the baseline was more reliably linear with RH795. With RH1691, the relation became linear above a certain level of baseline brightness (sqrt(F) = 28, which corresponds to 784/10,000 or 8% of the camera's range).

The excitation wavelength of RH795 coincides with the peak absorption of hemoglobin. Because this property may produce a blood flow-related signal,

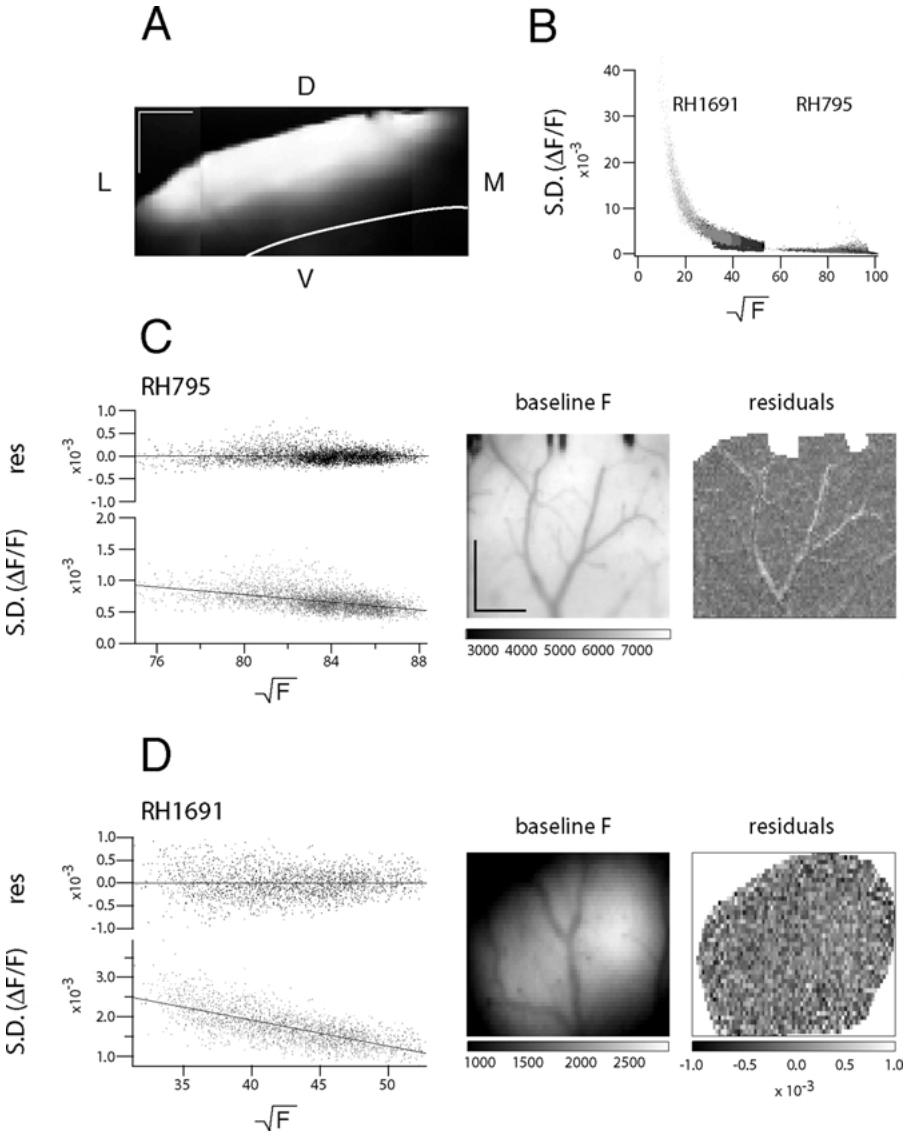

Fig. 1. Relation between brightness of stain and standard deviation of fractional fluorescence for RH795 and RH1691. (*A*) Coronal slice showing depth of dye penetration. Scale bars, 500 μm. (*B*) Plot of SD of fractional fluorescence against square root of baseline fluorescence at each pixel for 5 representative preparations for each dye.(*C, D*) *Left*: Data from selected single preparations in *B* with expanded scales, with residuals from linearity plotted on upper axis. *Right*: Maps of baseline fluorescence and residuals from linearity. Scale bars (500 μm) apply to all four maps.

which could compromise the neural signal, it has been cited as a major disadvantage of this dye (Shoham et al., 2001). To assess the degree to which this problem might impact recordings in this preparation, we examined the relation shown in Fig. 1*B* more closely, for a typical preparation with each dye.

Two of the data sets plotted in Fig. 1*B* are plotted separately in Fig. 1*C* and *D*, with the axes expanded. Above each plot, the residuals from linearity are shown. The fits to linearity are comparable (1*C*: Pearson's $R = -0.54$; 1 *D*: Pearson's $R = -0.67$); however, the distribution of residuals differs markedly. The distribution of the RH795 residuals is biased toward positive values, indicating a population of pixels with a larger standard deviation than the baseline fluorescence would predict. By contrast, for the RH1691 preparation, the residuals distribute evenly on both sides of 0. To the right of Fig. 1*C* and *D*, the residual values are mapped. The maps clearly show that the deviations from the shot-noise line with RH795 were associated with the blood vessels, which are visible on the cortical surface in the baseline fluorescence image. No such spatial structure of residuals was visible in the RH1691 recording (Fig. 1*D*).

We noticed that the perturbations in the noise level in the RH795 signal caused by the blood vessels were only a small number of the total pixels, while the brightness of staining was much better in most cases, as shown in the examples of Fig. 1*B*. Figure 2*A* shows a portion of the fluorescence background from an RH795 preparation, with a series of single-pixel recordings from this preparation of the response to a whisker deflection. In the left panel, "near vessel," the pixels are chosen from the area immediately overlaying a major blood vessel, indicated by open squares in the image. In these signals, the prestimulus baseline is not consistently flat, and the neural response is embedded in a slow signal which is

extremely variable over several hundred milliseconds following the stimulus. The right panel, labeled "not near vessel," contains signals from single pixels located less than 100 μm away from the pixels in the left column, indicated in the image by closed squares. These signals show a flat prestimulus baseline and a rapid return to this baseline following the response. The near-vessel signals are clearly inferior for purposes of measuring neuronal activity. Below the panels, the averages of the traces in each are shown in register with the average VSD signal from the barrel-sized region indicated on the image. We note that the first 100 ms of the "near vessel" averaged signal does capture a response with the same latency and amplitude as the average of the "flat" signals. The spatially averaged signal, despite including a large portion of the blood vessel and many of the signals from the left column, shows a stable baseline and a response with the kinetics expected of an averaged postsynaptic potential, virtually indistinguishable from the "not near vessel" signals. The blood vessel-associated signal is manifested in these types of averaged signals mainly as an incomplete return to baseline following the neuronal response.

Analogous plots for an RH1691 experiment are shown in Fig. 2*B*. As expected, the "near vessel" signals are indistinguishable from the "not near vessel" signals. Notably, both the standard deviation and the signal size are larger in the RH1691 experiment (note that the vertical scale in 2*B* is compressed tenfold relative to that in 2*A*), although the S/N ratio for the averaged signal is not appreciably different from that in the RH795 preparation (for the averaged signals S/N = 16 and 17, respectively). In this RH1691 recording and others, the larger fractional fluorescence change seen in response to the stimulus is offset by the larger standard deviation in the noise, which is correlated to the weaker staining observed with this dye. We expect that, with improved staining, the standard deviation could be driven lower in order to realize the gains in S/N that have been demonstrated in other reports (Shoham et al., 2001, Petersen & Sakmann 2003). Nevertheless, we note that over columnar and subcolumnar spatial scales several times larger than the blood-vessel diameter, or for single pixels chosen with attention to the vasculature, the signal-to-noise provided by RH795 is more than adequate for spatiotemporal analysis of cortical responses in mouse barrel cortex.

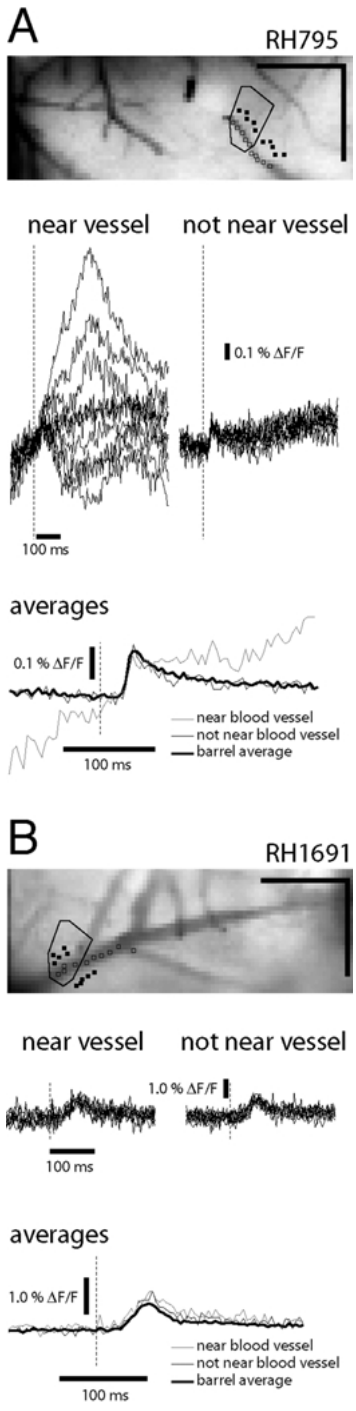

Fig. 2. Differential effect of vasculature on evoked response observed with RH795 and RH1691. (*A*) Background image from RH795 staining (contrast enhanced for clarity). Scale bars (500 μm) apply to images in *A* and *B*. Open squares indicate locations of "near vessel" pixels. Closed squares indicate locations of "not near vessel" pixels. Black open polygon indicates the border of a barrel visualized post-hoc in layer 4 with cytochrome oxidase histology. (*B*) Same as *A*, except data is from an RH1691 preparation. For simplicity, the same barrel outline is used. For traces, horizontal scale bar is 100 ms; vertical scale bar is 0.1% $\Delta F/F$ in *A*, 1.0 % $\Delta F/F$ in *B*.

Spatiotemporal Properties of Electrically vs Whisker-evoked Responses

We next sought to determine how the spatiotemporal properties of responses evoked by sensory stimulation compared to those evoked by electrical stimulation of the cortex. Both types of stimulation produced pop-

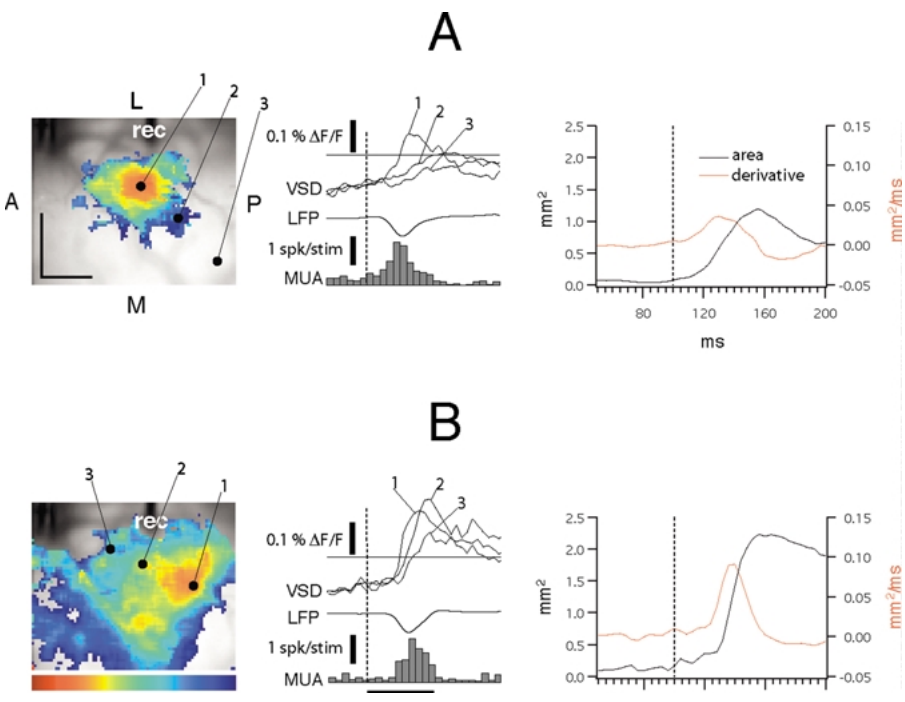

Fig. 3. Comparison of responses to single and multiple whisker stimuli. *Left*: maps represent the response onset latency according to the pseudocolor scale below the map in 3*B*. Scale bars, 500 μm. *Center*: Traces show the relative timing of the VSD signals from the pixels indicated by black solid circles on the latency maps, as well as the LFP and MUA signals recorded on the electrode marked "rec." Horizontal scale bar: 100 ms. Vertical scale bars: for VSD traces, 0.1% $\Delta F/F$, for MUA histogram, 1 spike/trial. VSD signal level at which response latency was measured is indicated by the horizontal line through the VSD traces. *Right*: Plots of significantly activated area as a function of time (*black*) and the derivative of this function (*red*). Stimulus time is indicated by the vertical dotted line.

ulation activity in the supragranular cortical network, which spread over thousands of μm^2. Representative responses to two types of whisker stimulation in the same preparation are shown in Fig. 3. Figure 3*A* shows the response to a 100 ms ramp-and-hold deflection (rise time 8 ms, velocity 1300 deg/s) of whisker C3. On the maps at left, pixels showing a response to the stimulus are pseudocolored according to the onset latency at that location (*see* calibration bar below left panel in *B*). The earliest response is seen at ~24 ms in a single discrete region 300 μm in diameter. The response propagated in all directions but preferentially in the posteriomedial direction. This can also be seen by comparison of the VSD signal from the single pixels marked with solid circles (middle column, "VSD"). The horizontal line indicates the threshold used to determine which pixels were included in the latency map. We calculated a point-to-point propagation velocity of 30 mm/s between points 1 and 2. On the same time scale, the LFP and MUA activity recorded from the electrode marked "rec" are shown. The responses recorded from the electrode lead the VSD response by a few (< 4) ms, presumably reflecting the greater contribution of layer 4 to the LFP signal relative to the VSD signal.

Figure 3*B* shows the response to a 10 ms, 6 PSI air puff delivered to whiskers C1 and D1. This multiwhisker response occupied a much larger area. Again, the signals shown from single pixels were used to calculate point-to-point propagation velocities of 196 mm/s from 1 to 2 and 73 mm/s from 2 to 3. Propagation velocity decreased as distance from the epicenter of the response increased. It is important to note that point-to-point velocity measurements are sensitive to the signal level at which arrival times are measured, with higher choices of threshold tending to produce larger time differences and, therefore, slower velocities, since the initial slope of the response decreases as the signal propagates (refer to traces in center panels of Figs. 3 and 4).

In order to compare the cortical area activated by stimuli across experiments, we computed the significantly responding area as a function of time (black traces, at right, *see* Methods). The derivative of this function (red traces, mm^2/ms) measures how quickly cortical area was recruited to participate in the response. Taken together, the peaks of the area function and its derivative, and the times at which these peaks occur, concisely summarize the spatiotemporal development of an evoked response. For the example shown in Fig. 3*A*, at 30 ms poststimulus, the expansion rate of the area peaked at 0.036 mm^2/ms and the peak area of 1.19 mm^2 was reached at 55 ms poststimulus. For the larger response shown in Fig. 3*B*, the expansion rate of the area peaked at 0.091 mm^2/ms at 40 ms after the stimulus, and the peak area of 2.23 mm^2 was reached at 55 ms.

Electrical stimuli to the cortex evoked a corresponding range of VSD response extents. Figure 4 shows two recordings from a different experiment, of responses to electrical stimulation at different amplitudes. The intensities of stimulation were 0.1 (4*A*, top) and 0.2 (4*B*, bottom) mA. The figure layout is identical to Fig. 3. On the onset-latency maps at left, the stimulation and recording electrodes are indicated by "stim" and "rec" respectively. Typical

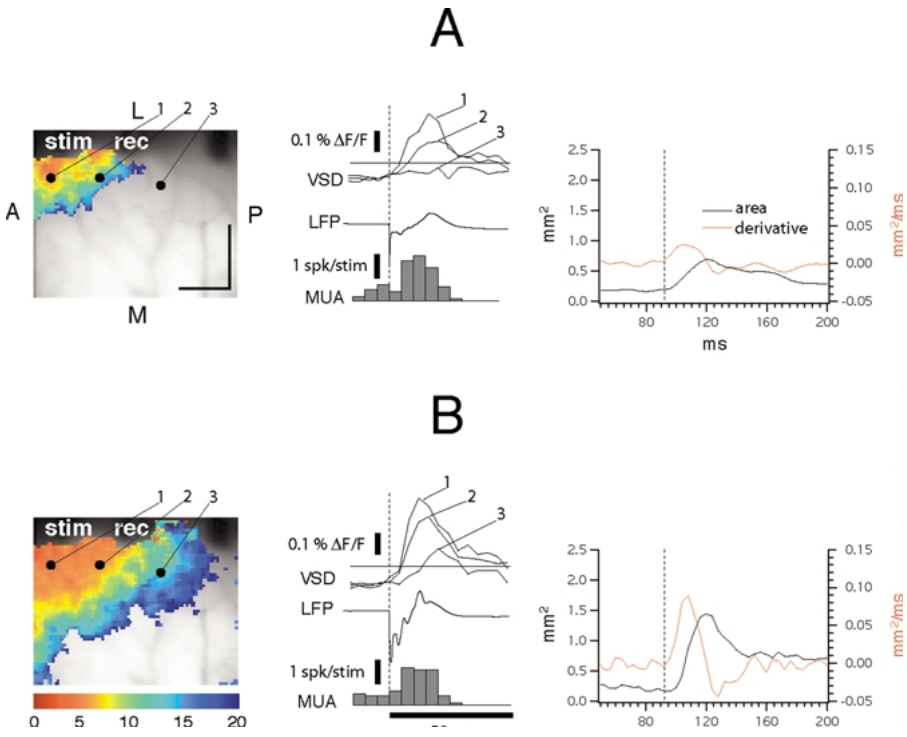

Fig. 4. Comparison of responses to low amplitude (*A*) and high amplitude (*B*) electrical stimuli. Stimulating electrode is marked "stim." *Left*: Maps represent the response onset latency according to the pseudocolor scale at the bottom. Scale bars, 500 μm. *Center*: Traces show the relative timing of the VSD signals from the pixels indicated by black solid circles on the latency maps, as well as the LFP and MUA signals recorded on the electrode marked "rec." Horizontal scale bar: 100 ms. Vertical scale bars: for VSD traces, 0.1% $\Delta F/F$, for MUA histogram, 1 spike/trial. VSD signal level at which response latency was measured is indicated by the horizontal line through the VSD traces. *Right*: Plots of significantly activated area as a function of time (*black*) and the derivative of this function (*red*). Stimulus time is indicated by the vertical dotted line.

of direct activation of the cortex, the shortest onset latencies appear instantaneous at this time resolution (4 ms/frame). As with the whisker responses shown in Fig. 3, we used signals from single pixels to compute point-to-point propagation velocities. For the low-amplitude stimulus the velocity from point 1 to 2 was 101 mm/s; no value could be computed from 2 to 3 due to the lack of response at 3. For the high-amplitude stimulus the velocity from point 1 to 2 was 121 mm/s; the velocity from point 2 to 3 was 56 mm/s. The velocity values obtained with electrical stimulation were in the same range as those obtained from whisker stimulation. For both types of stimulation, the values at the higher end of the range agree well with previously reported values of wave propagation speed observed with VSDs in the upper cortical layers in mouse thalamocortical slices (112 mm/s (Laaris, Carlson, & Keller, 2000)), mouse cortical slices cut along bowel rows (130 mm/s (Laavis & Keller, 2002)), guinea pig sensory cortial slices (181 ± 44 mm/s, (Contreras & Llinas, 2001), and rat sensory cortical slices (150–160 mm/s, (Haupt, 2000)). These velocities reported here are significantly slower than those computed by a different method from VSD responses to auditory and electrical stimulation in the guinea pig auditory cortex in vivo (380 mm/s and 260 mm/s (Song et al., 2005)). This difference could be attributed to our use of bipolar stimulating electrodes, which could engage more intracolumnar inhibition.

As seen with different intensities of whisker stimulation, both the responding area and the peak rate at which this area grew increased with stimulus intensity. The weaker stimulus activated a peak area of 0.70 mm^2, reached at 20 ms poststimulus, at a peak expansion rate of 0.025 mm^2/ms, which was attained at 5 ms poststimulus. The stronger stimulus activated a peak area of 1.44 mm^2, reached at 20 ms poststimulus, at a peak expansion rate of 0.089 mm^2/ms, reached at 8 ms poststimulus. Because the stimulus current density is greatest between the two poles of the electrode, the increased area activated by the stronger stimulus likely reflects direct activation of more cells and horizontal fibers there, followed by greater resultant activation postsynaptic to those elements.

The examples of Figs. 3 and 4 show that similarly-sized areas of barrel cortex can be activated with an overlapping range of expansion rates by whisker and electrical stimuli of varying magnitudes. To examine the relationship between the amount of area engaged by a stimulus and the peak rate at which that area was engaged, we plotted the peak of the area function's derivative against the peak of the area function itself for a large population of recordings ($n = 87$ recordings in 37 animals) in which stimulus amplitudes varied over a range corresponding to the range shown in Figures 3 and 4. This plot is shown in Figure 5, and includes data from RH1691 and RH795 experiments. For both whisker (*crosses*) and electrical stimuli (*circles*) there was a linear relationship between the two peaks, indicating that the amount of cortical area engaged by a response was linearly related to how fast the area was initially recruited. This relationship held whether the stimulus

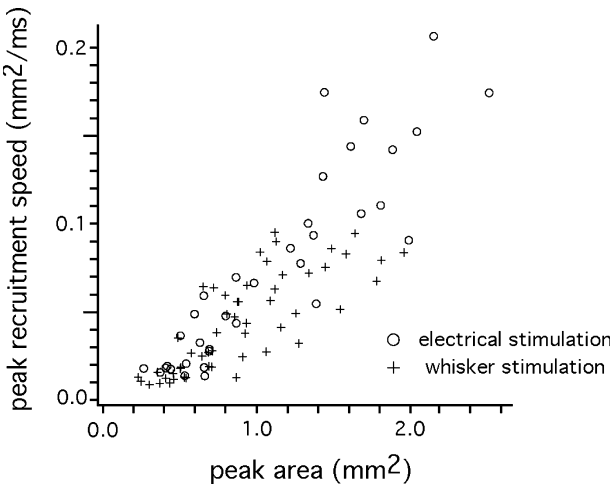

Fig. 5. Peak area recruitment speed plotted against peak area recruited. $n = 87$ recordings in 37 mice. Optical recordings were obtained in experiments with either RH795 or RH1691. *Circles*: electrical stimuli; *crosses*: whisker stimuli.

arrived from the whiskers via the thalamus, or whether the stimulus was delivered directly to the cortex by means of nonspecific electrical activation. Another notable feature of the graph is the substantial overlap in the values of the two parameters for both types of stimuli.

The exception to this is the population of higher expansion rates (> 0.1 mm^2/ms, $n = 11$) occasionally observed under electrical stimulation. Point-to-point velocities greater than 300 mm/s were often observed in these recordings. While the agreement of response parameters indicates that some fundamental patterns of cortical activation may be stimulus-independent, the recruitment of area by electrical stimuli at a rate outside the range of even the strongest whisker stimuli indicates that caution should be used when applying direct electrical stimulation to explore properties of cortical networks. We suggest that point-to-point velocities as well as speed of area recruitment be employed as considerations when assessing the relevance of an electrically-evoked response to the normal function of cortical networks.

The overlap in the ranges of the area function peaks is particularly striking in light of the contrasting widths of the impulses producing the cortical response in the two situations (electrical vs whisker). Figure 6 shows 2 representative thalamic multiunit responses to single ramp-and-hold whisker deflections, as well as the corresponding peristimulus time histogram (PSTH) ($n = 30$ trials) from those recordings.

Both thalamic response peaks are 10 ms wide at half-height, with additional activity continuing for 40–100 ms after the stimulus. In the upper example, a prominent "off" response is present, which is 30 ms wide at half height. In the lower example, a tonic

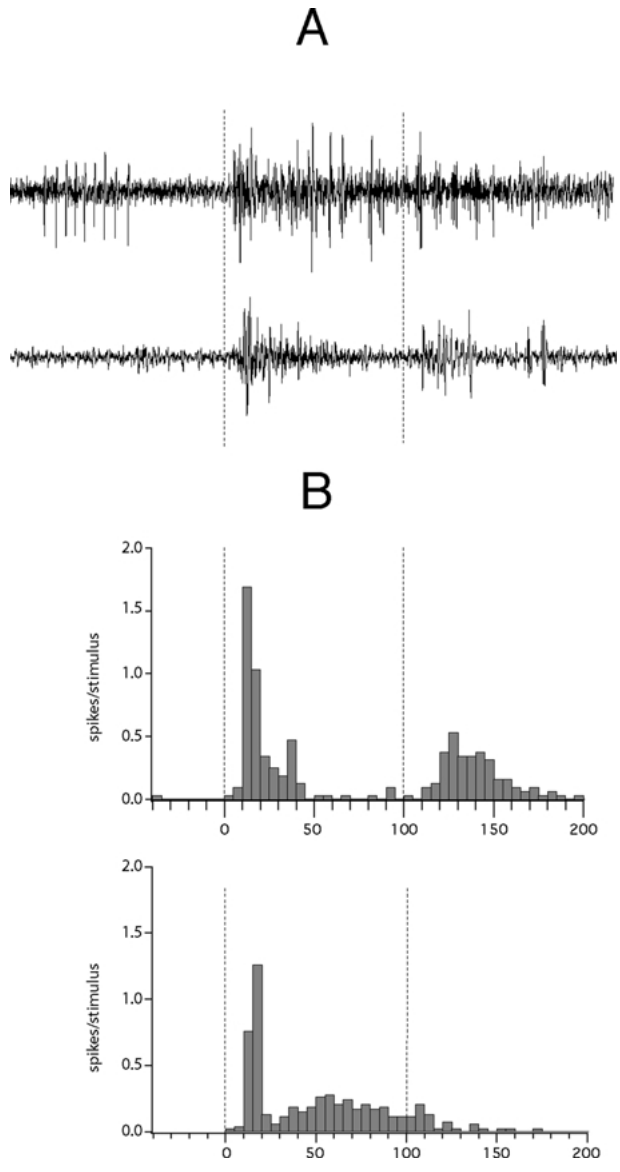

Fig. 6. Multi-unit responses to whisker deflection recorded in the thalamus. (*A*) Examples of single trial responses in two preparations, bandpass-filtered between 300 and 10,000 Hz. (*B*) Multi-unit PSTHs constructed from the recordings shown in *A* and *B*.

response continues for 100 ms after the phasic response. In contrast to these thalamic drives, electrical stimuli to the cortex were 0.1 ms in duration, or 2 orders of magnitude shorter. In light of this, it is remarkable that a correction for the arrival time to the cortex should be all that is necessary to match the time courses of the population responses at a coarse level of detail. The correspondence indicates that, to a significant degree, propagation of excitation is a corticocortical phenomenon, which is independent of the initiating mechanism.

The correspondences described above indicate similarity in the spatiotemporal properties of whisker- and electrically-evoked responses; however, we observed important differences under a paired-pulse

stimulation regime. Figure 7 shows the result of the presentation of pairs of whisker and electrical stimuli. The fluorescence background image is shown at the top, with histologically identified barrels from layer 4 superimposed. For the paired whisker stimulation, the stimulated whisker was C3. For electrical stimulation, electrical stimuli were delivered from the electrode marked "stim." Column-averaged VSD traces are shown from the C3 barrel, as well as its row-neighbors C2 and C4, and its arc-mates, D3 and E3. LFP and MUA recordings from the electrode marked "rec" are shown below the corresponding VSD traces.

Paired-pulse depression of the whisker responses was observed in the VSD traces at both frequencies. Paired pulse ratios (PPRs) for the 5 barrel columns are shown at the right. Depression was greater at 10 Hz (*continuous lines*), with PPRs ranging from 0.23–0.51 vs 0.54–0.77 at 4 Hz (*dotted lines*). At both frequencies, PPRs were lower outside the C row (*empty symbols*) than inside the C row (*filled symbols*). In other words, the principal barrel and its row-neighbors followed both pairs of stimuli, but especially the 10 Hz pair, more closely than barrel columns outside the row. This is consistent with stronger connections along a row than along an arc (Bernardo et al., 1990). The similarity between the C3 and C4 column responses and their difference from the D3 and E3 responses can be seen clearly in the VSD traces at the left. In contrast to the VSD signals, very little alteration in the second response was seen in the LFP or MUA at either frequency.

In contrast to the paired whisker stimuli, paired electrical stimuli produced miminal paired-pulse depression of the VSD, LFP, and MUA responses. PPRs as low as 0.65 were observed at 4 Hz in the D3 and C2 barrel-columns; however, for all other locations at both frequencies the values ranged from 0.8–1.1. The greater degree of paired-pulse depression observed with electrical stimuli relative to whisker stimuli is consistent with our observations in many such recordings ($n > 30$).

Discussion

We have examined the spatial structure of the noise in recordings using two commonly-used styryl dyes, applied topically in adult mouse somatosensory cortex, and report that the signal-to-noise limitations of RH795 can be minimized by attention to the vasculature. In addition, we report that electrical stimuli of low to moderate amplitude can successfully mimic the spread of activation seen with physiological stimuli in barrel cortex; however, high-amplitude electrical stimuli may produce responses with unrealistic spatiotemporal parameters. Propagation of single responses in cortical networks is largely independent of the method of activation, but paired responses show varying degrees of depression, depending on the activation method.

Response Properties

The peak area recruited by a stimulus was shown to be linearly related to the peak speed at which area was recruited during the development of the response. It is important to note that this does not necessarily need to be the case. The existence of this relationship has implications for the spatiotemporal development of cortical activation. On one hand, the time course of evoked responses in the cortex outlasts the duration of the stimulus by tens to hundreds of milliseconds, which implies some degree of persistent activity. On the other hand, this activity is under constraint, as neither electrical nor whisker stimulation was observed to initiate a runaway process in which, for example, the recruited area grew slowly at first, and then faster, eventually reaching the maximum observable area. This balance may be a fundamental property of input arrival in the supragranular cortex, a result of the dominance of inhibition over excitation and the precise relative timing dictated by the cortical circuitry.

Limitations of Area Measurements

The measurements of activated area and area recruitment speed allow the reduction of a three-dimensional data set (an optical recording) to two characteristic parameters, which can be compared across different types and intensities of stimulation, provided an equal amount of cortex is theoretically accessible to the stimulus in each case (here, a requirement for inclusion in our data set). This is advantageous; however, we note that there are many important spatiotemporal properties of a response not captured by these parameters. Paramount among them are the path taken by the excitation as it spreads, and the distribution of response amplitudes over space and time. These fundamental questions can be most directly assessed using VSDs, and are the subject of ongoing work in our laboratory (Civillico and Contreras, in preparation).

Relationship of Area Expansion Rate to Point-to-Point Velocity

An additional limitation of measurements based on activated area is that, unlike measurement of point-to-point propagation velocity for example, they are not directly related to physiological characteristics of single cells, and thus provide limited information about underlying mechanisms of observed phenomena. We note that the measurement of area recruitment speed employed here may be theoretically

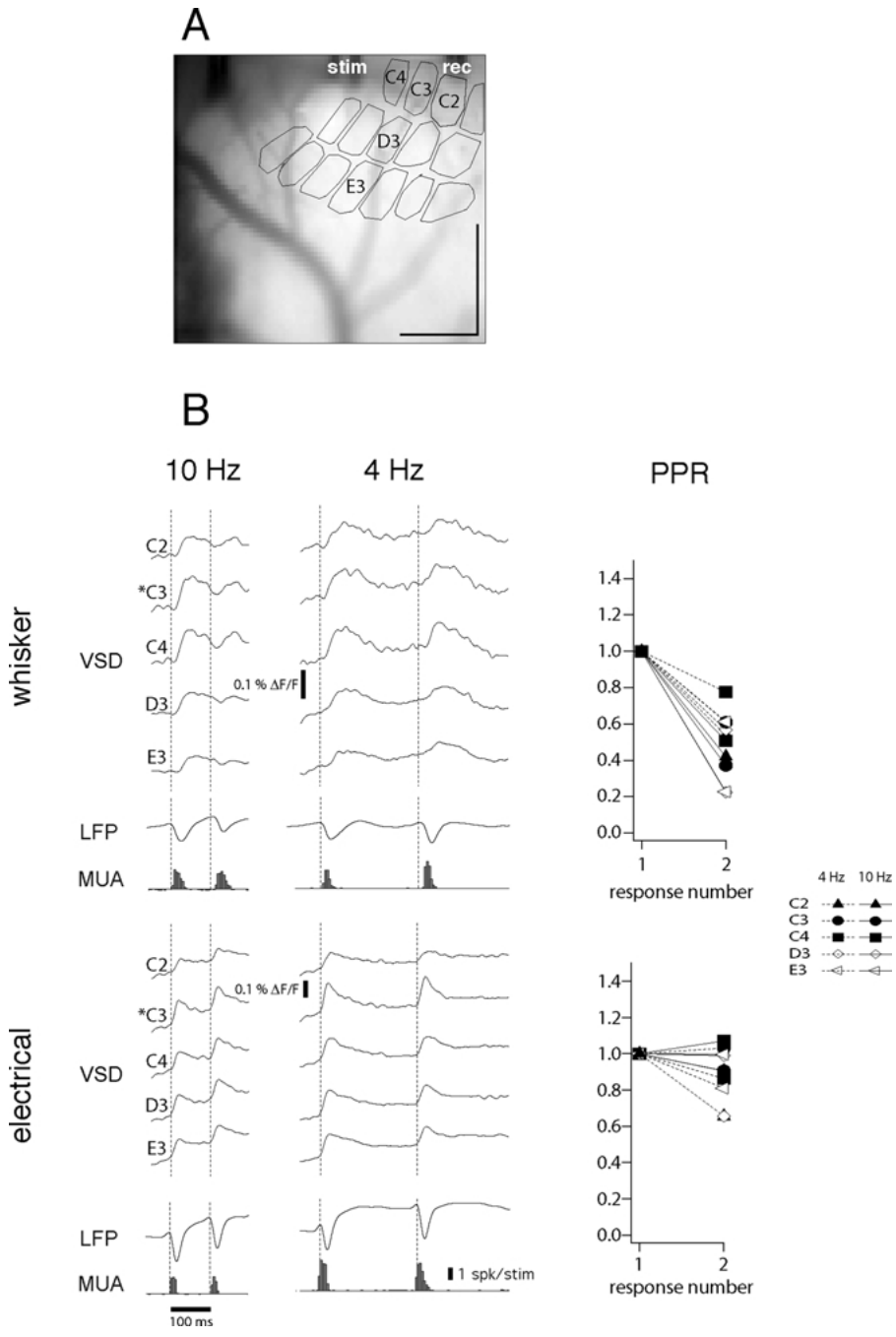

Fig. 7. Paired-pulse ratios of whisker- and electrically-evoked responses. (*A*) Background fluorescent image with superimposed barrel field determined from histology and aligned using fiducial marks (*not shown*). Stimulating and recording electrodes labeled "rec" and "stim." Scale bars, 500 μm. (*B*) *Left*: Time-aligned traces show simultaneous VSD, LFP and MUA signals recorded from the locations shown in response to 10 Hz and 4 Hz pairs of whisker (*top*) and electrical (*bottom*) stimuli. Vertical scale bars: 0.1% $\Delta F/F$ for VSD traces, 1 spike/trial for MU histograms. Horizontal scale bars: 100 ms. PPR values (response 2 / response 1) are quantified at right for five barrel-columns.

related to propagation velocity as follows: Assuming a circular response with radius r increasing at a constant rate (analogous to propagation velocity), the rate of growth of the area A is related to the radius and its rate of growth by $dA/dt = 2\pi r(dr/dt)$. For the single whisker response in Fig. 3*A* the peak area expansion rate was 0.036 mm^2/ms. At the time this rate occurred, the size of the activated area was 0.57 mm^2. Using the above equation, the theoretical point-to-point velocity at any point on the edge at that time is 14 mm/s, close to the value of 30 mm/s which was computed for this response using representative single pixel traces (*see* Results section). While the approximation of a single-whisker-evoked response as an expanding circle is obviously imperfect, the reasonable agreement between theoretical and observed velocity values provides some justification for relating the area expansion rate to the propagation velocity away from the response epicenter.

Very Rapidly Propagating Responses

The comparison of spatiotemporal parameters of whisker and electrically-evoked responses indicates

that electrical stimuli may evoke responses in cortex that are "realistic" according to the limited metrics employed here. However, we also observed, in the highest-amplitude cases, electrically-evoked responses that grew in area more rapidly than any response seen with whisker stimulation. These responses may be caused by activation of a greater density of horizontal fibers than would be recruited by a physiological stimulus, or they may represent a non-physiological form of activation, such as antidromic activation of axons. We cannot rule out the possibility that minute variations in the orientation or depth of electrodes from one experiment to another might increase the chances of observing such responses. We suggest that the interpretation of electrically-evoked responses can be made more straightforward by controlling for the parameters measured here.

Methodological Considerations

The advantages of VSDs over traditional electrophysiological methods are many. VSDs act as relatively noninvasive, minimally damaging probes of averaged subthreshold membrane potential changes over thousands of neuronal elements in a network. Their use allows the targeting of regions of interest of arbitrary size and shape. The balance between spatial resolution and signal-to-noise ratio can be adjusted to suit the question; continuing advances in probe design will reduce the need for such a choice. Here, we have corroborated the reports of decreased sensitivity to vascular artifacts of RH1691 relative to RH795; however, we have also shown that the contamination of the neural signal by blood-related signal in our preparation is limited to an area immediately adjacent to the blood vessels, and that high-signal recordings can be obtained from 529 μm^2 areas (single pixel, under our conditions) as little as 50 μm away from the vessels. We have further shown that, for areas the size of a barrel-column, the contribution from vessel-contaminated pixels has a minimal effect on the averaged signal. If desired, such pixels can easily be eliminated before analysis by screening the residuals from the relation plotted in Fig. 1. In our hands, RH795 has a greater affinity for adult mouse barrel cortex than RH1691, and we have found that its brighter, more reproducible and even stain more than compensates in yield for occasional vascular artifacts.

Sponsored by The Human Frontier Science Program Organization and the David and Lucille Packard Foundation. The authors are grateful to Esther Garcia de Yebenes for histology.

References

Bernardo, K.L., McCasland, J.S., Woolsey, T.A., Strominger, R.N. 1990. Local intra- and interlaminar connections in mouse barrel cortex. *J. Comp. Neurol.* **291:**23l–255

Cohen, L.B., Salzberg, B.M. 1978. Optical measurement of membrane potential. *Rev. Physiol. Biochem. Pharmacol.* **83:**35–88

Cohen, L.B., Salzberg, B.M., Grinvald, A. 1978. Optical methods for monitoring neuron activity. *Annu. Rev. Neurosci.* **1:**171–182

Contreras, D., Durmuller, N., Steriade, M. 1997. Absence of a prevalent laminar distribution of IPSPs in association cortical neurons of cat. *J. Neurophysiol.* **78:**2742–2753

Contreras, D., Llinas, R. 2001. Voltage-sensitive dye imaging of neocortical spatiotemporal dynamics to afferent activation frequency. *J. Neurosci.* **21:**9403–9413

Contreras, D., Steriade, M. 1995. Cellular basis of EEG slow rhythms: a study of dynamic corticothalamic relationships. *J. Neurosci.* **15:**604–622

Creutzfeldt, O.D., Watanabe, S., Lux, H.D. 1966. Relations between EEG phenomena and potentials of single cortical cells. I. Evoked responses after thalamic and erpicortical stimulation. *Electroencephalogr. Clin. Neurophysiol.* **20:**1–18

Devor, A., Dunn, A.K., Andermann, M.L., Ulbert, I., Boas, D.A., Dale, A.M 2003. Coupling of total hemoglobin concentration, oxygenation, and neural activity in rat somatosensory cortex. *Neuron* **39:**353–359

Erinjeri, J.P., Woolsey, T.A. 2002. Spatial integration of vascular changes with neural activity in mouse cortex. *J. Cereb. Blood Flow Metab.* **22:**353–360

Gil, Z., Connors, B.W., Amitai, Y. 1997. Differential regulation of neocortical synapses by neuromodulators and activity. *Neuron* **19:**679–686

Gil, Z., Connors, B.W., Amitai, Y. 1999. Efficacy of thalamocortical and intracortical synaptic connections: quanta, innervation, and reliability. *Neuron* **23:**385–397

Goldreich, D., Peterson, B.E., Merzenich, M.M 1998. Optical imaging and electrophysiology of rat barrel cortex. II. Responses to paired-vibrissa deflections. *Cereb. Cortex* **8:**184–192

Grinvald, A., Lieke, E.E., Frostig, R.D., Hildesheim, R. 1994. Cortical point-spread function and long-range lateral interactions revealed by real-time optical imaging of macaque monkey primary visual cortex. *J. Neurosci.* **14:**2545–2568

Haupt, S.S. 2000. Optical recording of spatiotemporal activation of rat somatosensory and visual cortex in vitro. *Neurosci. Lett.* **287:**29–32

Kleinfeld, D., Delaney, K.R. 1996. Distributed representation of vibrissa movement in the upper layers of somatosensory cortex revealed with voltage-sensitive dyes. *J. Comp. Neurol.* **375:**89–108

Konnerth, A., Obaid, A.L., Salzberg, B.M. 1987. Optical recording of electrical activity from parallel fibres and other cell types in skate cerebellar slices in vitro. *J. Physiol.* **393:**681–702

Laaris, N., Carlson, G.C., Keller, A. 2000. Thalamic -evoked synaptic interactions in barrel cortex revealed by optical imaging. J Neuosci 20:1529–37

Laaris, N., Keller, A. 2002. Functional independence of layer IV barrels. J Neurophysiol 87:1028–1034

Masino, S.A., Kwon, M.C., Dory, Y., Frostig, R.D. 1993. Characterization of functional organization within rat barrel cortex using intrinsic signal optical imaging through a thinned skull. *Proc. Natl. Acad. Sci. USA* **90:**9998–10002

Morin, D., Steriade, M. 1981. Development from primary to augmenting responses in the somatosensory system. *Brain Res.* **205:**49–66

Obaid, A.L., Loew, L.M., Wuskell, J.P., Salzberg, B.M. 2004. Novel naphthylstyryl-pyridium potentiometric dyes offer advantages for neural network analysis. *J. Neurosci. Methods* **134:**179–190

Petersen, C.C., Grinvald, A., Sakmann, B. 2003a. Spatiotemporal dynamics of sensory responses in layer 2/3 of rat barrel cortex measured in vivo by voltage-sensitive dye imaging combined with whole-cell voltage recordings and neuron reconstructions. *J. Neurosci.* **23:**1298–1309

Petersen, C.C., Hahn, T.T., Mehta, M., Grinvald, A., Sakmann, B. 2003b. Interaction of sensory responses with spontaneous depolarization in layer 2/3 barrel cortex. *Proc. Natl. Acad. Sci. USA* **100:**13638–13643

Salzberg, B.M. 1989. Optical recording of voltage changes in nerve terminals and in fine neuronal processes. *Annu. Rev. Physiol.* **51:**507–526

Salzberg, B.M., Obaid, A.L., Senseman, D.M., Gainer, H. 1983. Optical recording of action potentials from vertebrate nerve terminals using potentiometric probes provides evidence for sodium and calcium components. *Nature* **306:**36–40

Shoham, D., Glaser, D.E., Arieli, A., Kenet, T., Wijnbergen, C., Toledo, Y., Hildesheim, R., Grinvald, A. 1999. Imaging cortical dynamics at high spatial and temporal resolution with novel blue voltage-sensitive dyes. *Neuron* **24:**791–802

Song, W.J., Kawaguchi, H., Totoki, S., Inoue, Y., Katura, T., Maeda, S., Inagaki, S., Shirasawa, H., Nishimura, M. 2005. Cortical intrinsic circuits can support activity propagation through an isofrequency strip of the guinea pig primary auditory cortex. *Cereb. Cortex* 10.1093/cercor/bhj018

Timofeev, I., Contreras, D., Steriade, M. 1996. Synaptic responsiveness of cortical and thalamic neurones during various phases of slow sleep oscillation in cat. *J. Physiol.* **494:**265–278

Wong-Riley, M. 1979. Changes in the visual system of monocularly sutured or enucleated cats demonstrable with cytochrome oxidase histochemistry. *Brain Res.* **171:**11–28

Woolsey, T.A., Van der Loos, H. 1970. The structural organization of layer IV in the somatosensory region (SI) of mouse cerebral cortex. The description of a cortical field composed of discrete cytoarchitectonic units. *Brain Res.* **17:**205–242

Yuste, R., Tank, D.W., Kleinfeld, D. 1997. Functional study of the rat cortical microcircuitry with voltage-sensitive dye imaging of neocortical slices. *Cereb. Cortex* **7:**546–558